

Observations of Ionospheric Cavities Generated by High-Power Radio WavesL. M. Duncan^(a)*Los Alamos National Laboratory, Los Alamos, New Mexico 87545*

J. P. Sheerin

KMS Fusion, Ann Arbor, Michigan 48106

and

R. A. Behnke

National Science Foundation, Washington, D.C. 20550

(Received 22 February 1988)

High-power hf electromagnetic waves have been used to generate large electron-density cavities in the night-time *F*-region ionospheric plasma. Previous modification experiments have described induced density perturbations of only a few percent. Here we report the first observations of density depletions exceeding 50%, extending hundreds of kilometers along the geomagnetic field. These cavities are thermally driven, with electron temperatures in the depletions increased by factors of 3 to 4. The depletion dynamics exhibits many of the characteristics associated with thermal cavitons.

PACS numbers: 94.20.Vv, 52.35.Mw, 52.40.Db

High-power electromagnetic radiation incident on a plasma, acting through the nonlinear ponderomotive force or collisional thermal forces, can generate self-consistent density-profile modifications resulting in strong spatial localization of the pump wave. These localized plasma-density cavities, when supported by trapped electromagnetic radiation or associated electrostatic plasma waves, behave as large-scale cavitons.¹ Cavity formation, evolution, and collapse have been observed during recent hf ionospheric modification experiments at the Arecibo Observatory.

Numerous previous hf ionospheric modification experiments have explored the wave-plasma interactive processes leading to nonlinear density perturbations and electric-field localization. Over small scale sizes, experiments have investigated the development of ponderomotive-driven parametric instabilities, generating enhanced ion-acoustic and Langmuir turbulence.² On meter scales, differential plasma heating is believed responsible for structuring of the ionospheric plasma near the hf reflection height, producing field-aligned coherent scattering.³ On kilometer scales, plasma striations and hf beam filamentation have been interpreted in terms of the thermal self-focusing instability.⁴ Recent theoretical⁵ and experimental⁶ investigations of the onset of nonlinear effects have also suggested the importance of small-scale caviton development at the hf reflection height. In all of these studies, the induced electron-density profile modification was observed to be only a few percent. Here we report the first direct observations of large hf-induced electron-density depletions. In addition to its application to the study of basic nonlinear wave-plasma interactions, the experimental capability to generate reproducibly such large density and tempera-

ture perturbations in the natural ionosphere offers exciting new opportunities for perturbational studies of the geophysical environment.

The data presented were obtained during ionospheric modification experiments conducted at the Arecibo Observatory. The geomagnetic dip angle is approximately 50°. The ionospheric critical frequency was typically 3.5–4 MHz. The hf pump wave was operated on a frequency of 3.175 MHz, ordinary-mode polarization. The transmitted power was 300 kW, radiated from a 4×8 inverted log-periodic array with an effective antenna gain of 23 dB, and yielding approximately 50 $\mu\text{W}/\text{m}^2$ incident power density at ionospheric *F*-region heights. The high-power perturbing radiation operated cw with on/off cycles of tens of minutes duration. The principal diagnostic was a 430-MHz incoherent backscatter radar, measuring high-resolution power profiles versus range. The radar uses the 305-m-diam spherical antenna, producing a steerable beam with half-power width of less than a kilometer at ionospheric heights.

Typical diagnostic radar measurements employed a 52- μs Barker coded radar pulse, with a 10-ms pulse repetition period and 500–5000 variable pulse integration. This produces 600-m resolution profiles every 5–50 s with statistical fluctuations of 1%–5%. The return profiles undergo range-square correction, noise subtraction, and calibration. In addition to power profiles, long-pulse radar measurements were taken recurrently. These observations used a 300- μs radar pulse to determine the scattered signal autocorrelation function, and to estimate directly the electron and ion temperatures with 45-km range resolution and several-minute integration times.

The backscattered radar power P_r is dependent on the

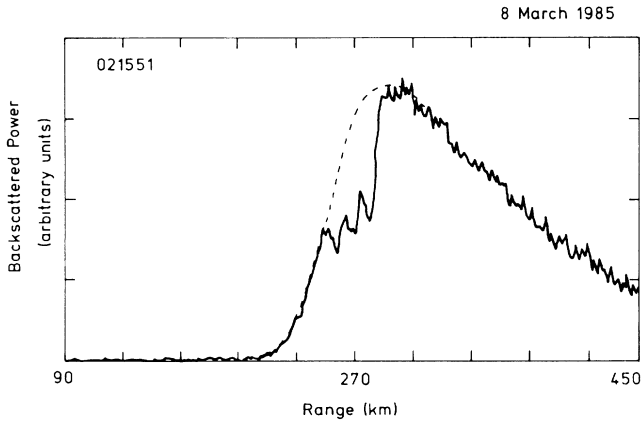


FIG. 1. Initial observation of large-scale ionospheric depletion. The hf radiated 200 kW cw beginning at 021146. The data shown are from a 1-min integration of 5000 radar pulses. The dashed curve approximates the undisturbed profile.

product of the electron density n_e and the effective electron scattering cross section σ_{eff} . This cross section is in turn dependent on the radar wavelength λ_r , the local plasma Debye length λ_D , the electron temperature T_e , and the ion temperature T_i , approximately expressed by⁷

$$\sigma_{\text{eff}} \sim \sigma_e (1 + T_r)^{-1} \text{ for } \alpha \ll 1,$$

where $\alpha = 4\pi\lambda_D/\lambda_r$, and $T_r = T_e/T_i$. The backscattered power is reduced by a decrease in the electron density or an increase in the electron-to-ion temperature ratio. A more exact treatment would also consider the enhanced ion-acoustic and electron plasma waves and non-Maxwellian electron velocity distributions expected within the modification region.⁸ Temperature perturbations typically respond on collisional Ohmic heating and conduction time scales of seconds, while macroscopic kilometer-scale density perturbations can develop in minutes and recover on diffusion time scales of tens of minutes or longer. We used this temporal scale difference to help distinguish thermal and density changes affecting the return radar power. As a first estimate, changes in the backscatter power profile occurring in the first minutes following hf on/off were assumed to be predominantly thermal effects, and profile modifications persisting for more than several minutes after hf turn-off were interpreted as primarily electron density changes. These results were then compared for consistency with explicit temperature measurements taken with substantially reduced resolution.

The initial observation of large ionospheric cavities is shown in Fig. 1. A series of cavities were observed to form below the hf reflection height, with a striking qualitative resemblance to the density cavities predicted in numerical simulations of strong electromagnetic wave interactions with nonuniform plasmas.⁹ However these numerical results considered the development of much smaller structures driven on short time scales by the non-

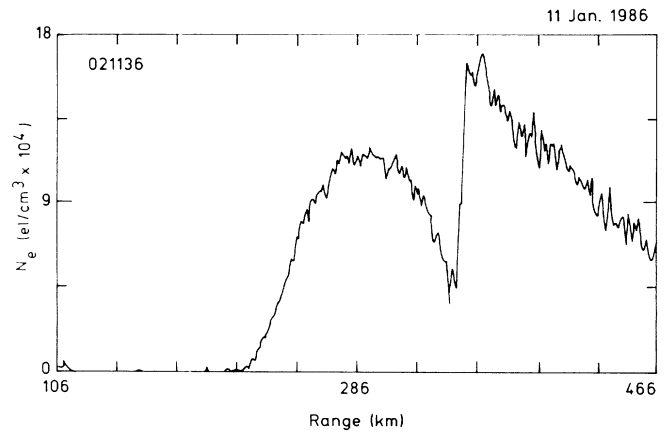


FIG. 2. Ionospheric profile showing typical steady-state hf-induced cavity. Long-pulse temperature measurements indicated $T_e/T_i \approx 3$ within the cavity, implying an electron-density depletion greater than 50%. The density scale is based on ambient calibration, and should be T_e/T_i adjusted.

linear ponderomotive force. Apparently, the observed ionospheric cavities may represent the same basic physical process, but driven by thermal forces acting on much longer spatial and temporal scales. Confirmation observations of these large hf-induced depletions were conducted during several subsequent experiments. Multiple cavity formations similar to those shown in Fig. 1 were found to be typical for developing stages of the disturbance. Moreover, the modified profile was observed to evolve reproducibly toward a characteristic steady-state disturbance, shown in Fig. 2. As a stable modified profile, a single deep cavity developed with temperature-corrected density depletions of greater than 50%. The large cavity exhibited substantial erosion of the hf reflection height into the ambient density gradient and sharp steepening of the upper cavity ledge. Density inventory estimates suggested that the depletions were pro-

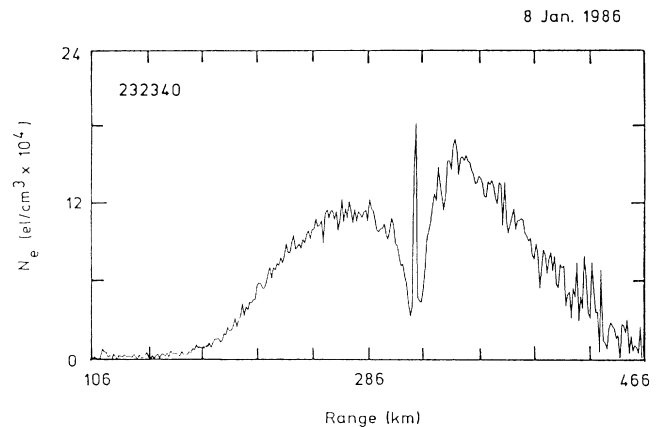


FIG. 3. Ionospheric profile showing hf-enhanced ion-acoustic waves excited at the base of the depletion cavity.

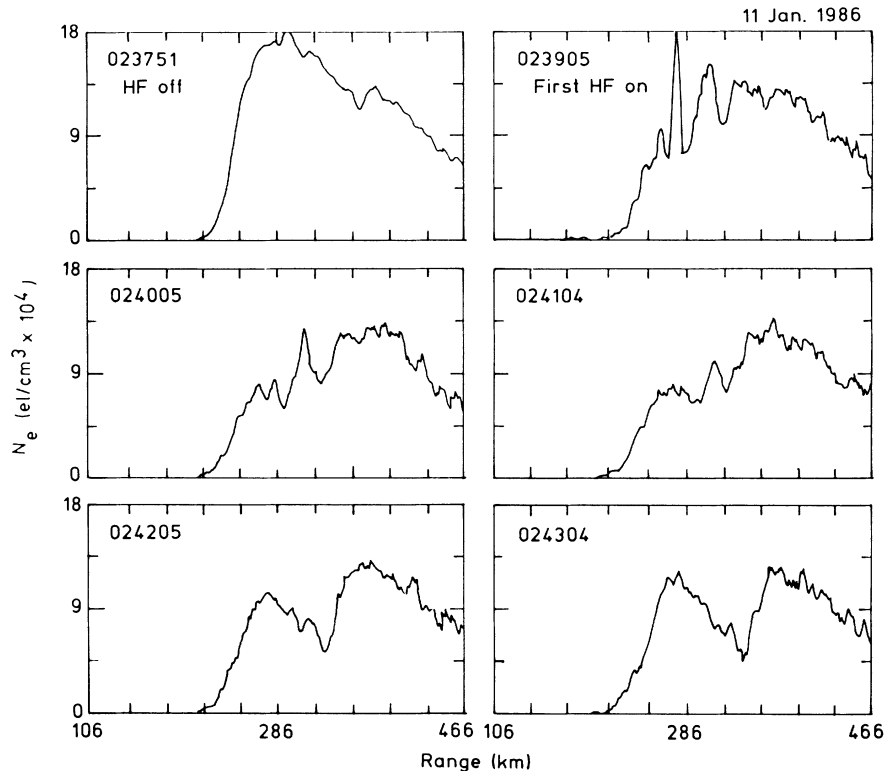


FIG. 4. Ionospheric profile sequence showing cavity development following hf turn-on at 0238. After 5 min, disturbance approaches steady-state cavity profile.

duced primarily by displacement of plasma along geomagnetic field lines, and not by locally enhanced recombination effects. Apparent trapping of the incident electromagnetic radiation was evidenced by the occasional observation of hf-enhanced ion-acoustic waves, typically associated with the parametric decay instability, as seen in Fig. 3. These waves were excited at the base of the depletion cavity.

Power-profile changes occurring in the first 2 min following hf turn-off were used to estimate the heating contribution to the reduced power returns. From this technique it was estimated that electron heating increased the electron-to-ion temperature ratio from an ambient value of $T_r \approx 1$ to a fully perturbed level of $T_r \approx 3-4$. The largest heating effects were observed to coincide with the locations of greatest density depletion. The estimates were in general agreement with results obtained by direct temperature measurements, with reduced spatial and temporal resolution. These observations indicated typical ambient temperatures of $T_e \approx T_i \approx 800$ K, and heated electron temperatures of $T_e \approx 2400$ K. The heated ion temperatures showed only minor increases, indicating as expected that they maintained locally good thermal contact with the neutral background. Several minutes after hf turnoff, electron temperatures had relaxed back to near ambient levels. Power profiles were converted to plasma densities on the assumption that $T_r \approx 1$.

Anomalous heating associated with collisional and Landau damping of parametrically enhanced Langmuir waves is believed to play a primary role in producing the observed thermally driven cavities. Extraordinary-polarization pump waves, which do not excite anomalous parametric heating, were found to produce only the modest temperature and density effects reported previously.

Time-dependent power profiles were used to study cavity development, evolution, and dissipation. The formative nonequilibrium stages of a large-scale cavity are shown in Fig. 4, presented at approximately 1-min intervals. The initial profile modification developed as a cascade of multiple structures of approximately 6-10-km horizontal scale, similar to the observation shown in Fig. 1. Enhanced ion-acoustic turbulence also was seen at the earliest times. Discrete cavity structures were observed to propagate independently along the density gradient with projected vertical velocities of 0-100 m/s, eventually coalescing into a single large cavity, approaching the characteristic steady-state configuration of Fig. 2. The evolving cavities exhibited many of the properties expected of large-scale thermal cavitons.¹⁰

Recovery of the ionospheric plasma following hf turn-off is presented in Fig. 5 in progressive 5-min intervals. The depletion appeared to recover in about 30 min. However, this was also approximately the time expected for the modified volume, moving at ionospheric plasma drift velocities, to traverse beyond the radar field of view,

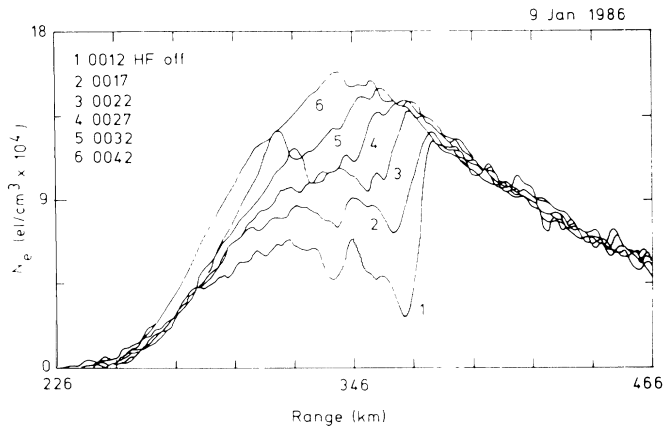


FIG. 5. Density profile recovery following hf turn-off at 0012.

suggesting that the induced depletions may in fact persist much longer than can be followed with fixed-radar diagnostics. The observed slow recovery is consistent with predictions for diffusive filling of large field-aligned ionospheric depletions.

Scanning of the radar beam along the magnetic meridian determined that the large depletions were highly field aligned. The range variation of the disturbance as a function of radar zenith angle was in good agreement with expectations based on field-aligned projections both above and below the hf interaction region. Typical horizontal scales of the large steady-state disturbances were comparable to the expected hf beam size of several tens of kilometers. In addition, the disturbance geometry appeared as depleted plasma sheets, as opposed to the filamentation rods associated with self-focusing.¹¹ Planar field-aligned depletions were observed extended for hundreds of kilometers above the modification region, essentially as far as the radar scanning could accurately follow the projected field line.

The special atmospheric conditions necessary for generation of large depletion cavities have not been determined. The depletions were observed reproducibly only after local midnight in the winter ionosphere, and for ionospheric densities critical only for the lowest pump frequency available, 3.175 MHz. At earlier pre-midnight times, for generally similar experimental conditions, heating effects of comparable magnitude were measured but usually accompanied by only moderate density reductions of approximately 10%. These modest effects were observed to recover to near ambient conditions in several minutes after hf turn-off. Seasonal dependence

has not yet been studied. Since large depletions were detected only after conjugate sunset, large-scale electrodynamic processes may play a contributing role, but do not appear sufficient to fully explain the observed temporal behavior. Expanded studies are continuing in attempts to determine what other special characteristics of the post-collapse ionospheric plasma also may be important to the generation of these large density cavities.

We wish to thank P. A. Bernhardt, F. T. Djuth, A. V. Gurevich, J. D. Hansen, and G. J. Morales for valuable discussions during the course of this research. The Arecibo Observatory is operated by Cornell University under contract to the National Science Foundation. This work was supported in part by a Los Alamos National Laboratory Institutional Support for Research and Development Grant.

^(a)Currently at Department of Physics and Astronomy, Clemson University, Clemson, SC 29634.

¹A. Y. Wong, *Phys. Scr.* **T2/1**, 262 (1982).

²J. A. Fejer, *Rev. Geophys. Space Phys.* **17**, 135 (1979), and references therein.

³P. A. Fialer, *Radio Sci.* **9**, 923 (1974); A. J. Coster et al., *J. Geophys. Res.* **90**, 2807 (1985).

⁴F. W. Perkins and E. J. Valeo, *Phys. Rev. Lett.* **32**, 1234 (1974); G. D. Thome and F. W. Perkins, *Phys. Rev. Lett.* **32**, 1238 (1974).

⁵J. P. Sheerin et al., *J. Atmos. Terr. Phys.* **44**, 1043 (1982); J. C. Weatherall et al., *J. Geophys. Res.* **87**, 823 (1982).

⁶A. Y. Wong et al., *Radio Sci.* **18**, 815 (1983); L. M. Duncan and J. P. Sheerin, *J. Geophys. Res.* **90**, 8371 (1985); W. Birkmayer, T. Hagfors, and W. Korman, *Phys. Rev. Lett.* **57**, 1008 (1986); A. Y. Wong, T. Tanikawa, and A. Kuthi, *Phys. Rev. Lett.* **58**, 1375 (1987); F. T. Djuth et al., *Geophys. Res. Lett.* **14**, 953 (1987).

⁷O. Buneman, *J. Geophys. Res.* **67**, 2050 (1962).

⁸H. C. Carlson and L. M. Duncan, *Radio Sci.* **12**, 1001 (1977); G. P. Mantas, H. C. Carlson, and C. A. LaHoz, *J. Geophys. Res.* **86**, 561 (1981); H. C. Carlson, V. B. Wickwar, and G. P. Mantas, *J. Atmos. Terr. Phys.* **44**, 1089 (1982).

⁹K. G. Estabrook, E. J. Valeo, and W. L. Kruer, *Phys. Fluids* **18**, 1151 (1975); G. J. Morales and Y. C. Lee, *Phys. Fluids* **20**, 1135 (1977); T. Tanikawa, A. Y. Wong, and D. L. Eggleston, *Phys. Fluids* **27**, 1416 (1984).

¹⁰K. B. Dysthe, E. Mjølhus, H. L. Pecseli, and K. Rypdal, *Phys. Scr.* **T2/2**, 548 (1982).

¹¹L. M. Duncan and R. A. Behnke, *Phys. Rev. Lett.* **41**, 998 (1978); D. T. Farley, C. LaHoz, and B. G. Fejer, *J. Geophys. Res.* **88**, 2093 (1983).